

Determination of bonding in diamond-like carbon by Raman spectroscopy

Andrea Carlo Ferrari*

Engineering Department, University of Cambridge, Cambridge CB2 1PZ, UK

Abstract

Raman spectroscopy is a very popular, non-destructive tool for the structural characterisation of carbons. Raman scattering from carbons is always a resonant process, in which those configurations whose band gaps match the excitation energy are preferentially excited. Any mixture of sp^3 , sp^2 and sp^1 carbon atoms always has a gap between 0 and 5.5 eV, and this energy range matches that of IR-vis-UV Raman spectrometers. The Raman spectra of carbons do not follow the vibration density of states, but consist of three basic features, the G and D peaks at approximately 1600 and 1350 cm^{-1} and an extra T peak, for UV excitation, at $\sim 980\text{--}1060\text{ cm}^{-1}$. We propose to rationalise the vast range of experimental data available in literature at any excitation wavelength by a simple model, which considers the main factors influencing the Raman spectra. The great advantages of multi-wavelength Raman spectroscopy will be clarified by a series of examples. In particular we show how it can be used to probe the structural changes induced by annealing and by nitrogen introduction. UV Raman spectroscopy also probes heteropolar σ bonds in a complementary way to infrared spectroscopy. We demonstrate the direct detection of C–H vibrations in hydrogenated DLC samples, Si–H and Si–C vibrations in amorphous silicon and amorphous silicon–carbon alloys and the easier probe of CN sp bonds in amorphous carbon nitrides. © 2002 Elsevier Science B.V. All rights reserved.

Keywords: Diamond-like carbon; Raman spectroscopy; Bonding; Structure

1. Introduction

Raman spectroscopy is a popular, non-destructive tool for structural characterisation of carbons [1–12]. It is traditionally carried out at the commonly available wavelengths in the blue–green spectral region (488–514.5 nm), but multi-wavelength Raman (MW Raman) studies are becoming increasingly used. Recently there has been a considerable improvement in the field of MW Raman spectroscopy in carbon systems. In particular, the appreciation of the strict correlation of the Raman process with the electronic properties of carbon systems is a major driving force to further develop all the possibilities of this versatile technique.

There are several examples of the present and prospective capabilities of Raman scattering. MW Raman has recently been used to distinguish the metallic and semiconducting forms of single wall carbon nanotubes [8,9]. We used it to investigate the origin of the peaks at $\sim 1150\text{ cm}^{-1}$ and $\sim 1450\text{ cm}^{-1}$ in nanocrystalline diamond [12] and it is also been used to study the metallic transition in highly boron doped diamond

[13,14]. Surface enhanced Raman spectroscopy (SERS) allows to attain up to 10^{12} enhancement factors [15,16]. It has been applied to single wall nanotubes [17,18], diamond [19,20] and amorphous carbon [20]. We also detected surface enhanced resonant Raman effects studying ultra-thin carbon films on Al [21]. SERS can thus be a powerful means to study local modifications in carbons. Scanning near field Raman spectroscopy allows in principle to obtain spatial resolutions down to $\lambda/20$ [22,23], where λ is the excitation wavelength. In order to get the highest resolution it should be applied to the shortest excitation wavelength; indeed, at the typical UV excitation of 244 nm one could attain ~ 12 nm spatial resolution [22,23]. In order to overcome the signal loss due to the small probe size of traditional SNOM, SERS and ‘aperture-less’ SNOM should be coupled [24]. In this approach an AFM tip is coated with (or made of) a metal, such as silver for visible excitation, and the laser light is directed onto this probe when in proximity of the sample, so to scatter Raman light from the near field. The metal probe can be chosen to optimise SERS at any excitation energy. This could lead to the realisation of a ‘nano-Raman’ or ‘Raman-

*Tel.: +44-1223-765242; fax: +44-1223-332662.

E-mail address: acf26@eng.cam.ac.uk (A.C. Ferrari).

AFM' instrument which could probe structural as well as morphological properties at the nanometre scale.

In this paper we review a model that we proposed to explain the trends of the Raman spectra of amorphous, disordered and diamond-like carbons at any excitation wavelengths. We particularly stress the advantages of the MW Raman analysis of the G peak. This peak is the easiest to detect and fit and the only one always present for the commonly used excitation energies. The dispersion of the G peak is a crucial parameter to distinguish samples that may exhibit very similar Raman spectra for a specific excitation energy, even if with different structure. Indeed, due to the linearity of the G peak dispersion with excitation wavelength, a simpler two-wavelength study can be enough to get the relevant information. We will then show a series of examples of how to use UV Raman spectroscopy for elemental detection. This is a largely unexplored field, which has high potential for development and application.

2. MW Raman spectroscopy

Unpolarised Raman spectra were acquired at different wavelengths between 229 and 785 nm (5.41–1.58 eV) using a variety of spectrometers. The power on the sample was kept well below 1 mW. Sample damage is always an issue in Raman measurements, but it is particularly serious for UV excitation. For H containing samples, in order to be sure that the signal we measured is a genuine feature, we performed measurements with samples rotating at a very high speed (>3000 rev./min) with a random XY movement superimposed. Fig. 1 shows the multi-wavelength Raman spectra of ta-C, ta-C:H, a-C and polymeric a-C:H samples [11].

The spectra in general show three features, at approximately 1560, 1360 (for visible excitation) and 1060 cm^{-1} (detected only in UV excitation), which are labelled as the G, D and T peaks, respectively. The G and D peaks are due to sp^2 sites only. The G peak is due to the bond stretching of all pairs of sp^2 atoms in both rings and chains [5]. The D peak is due to the breathing modes of rings. The T peak is due to C–C sp^3 vibrations and appears only for UV excitation. The G and T peaks trends are indicated in Figs. 2 and 3.

For visible excitation, the sp^2 sites have such a high cross-section that they dominate the spectra, the sp^3 sites are invisible and the spectrum responds only to the configuration or order of the sp^2 sites. As the excitation energy rises, two effects occur. Resonance causes the excitation of those sp^2 configurations with a wider gap. For deep UV the modes of σ states of C–C bonds are seen.

The films in Fig. 1 generally have a surface layer of lower density not exceeding 2 nm thickness [25], apart from the sputtered a-C, but in this case the bulk properties are not markedly different from the surface

ones [25]. Cross-sectional uniformity is crucial if we wish to relate UV Raman spectra to bulk properties, since UV excitation probes just the topmost ~ 10 – 15 nm of the samples at 224 nm. However, this surface sensitivity of UV Raman spectroscopy is ideal when we want to investigate the effects of surface treatments or ultra-thin films, such as those used for hard disk coating [21].

3. The G peak dispersion

The trends in the Raman parameters for different laser excitation can be rationalised by the three-stage model of bonding and ordering [5,11]. This considers an amorphisation trajectory, consisting of three stages from graphite to ta-C:

1. graphite \rightarrow nanocrystalline graphite (nc-G);
2. nanocrystalline graphite $\rightarrow \text{sp}^2$ a-C;
3. a-C \rightarrow ta-C ($\rightarrow 100 \text{ sp}^3$ ta-C, defected diamond).

The Raman spectra depend on

1. clustering of the sp^2 phase;
2. bond length and bond angle disorder;
3. presence of sp^2 rings or chains;
4. the sp^2/sp^3 ratio.

In visible Raman spectra the cross-section of the sp^2 phase is much higher (50–250 times for 514.5 nm) than the one of the sp^3 phase. Furthermore, the spectra directly depend on the quality or configuration of the sp^2 phase and only indirectly on the quantity of the sp^2 phase. Most times the sp^2 configuration varies consistently with the sp^2 fraction; however, in some cases, the sp^2 quality can be changed independently from the $\text{sp}^2:\text{sp}^3$ ratio. This phenomenon, which we called hysteresis [5], typically happens for high temperature deposition, annealing after deposition, low dose ion implantation of ta-C or unfiltered deposition processes. Fig. 2 shows the trends in the G and D peaks for the three stages for 514.5 nm excitation [5]. Broadly, stage 1 corresponds to the reduction of the in-plane correlation length L_a within an ordered graphite layer. The average G peak position moves from 1581 cm^{-1} to ~ 1600 cm^{-1} due to phonon confinement in smaller graphitic domains, since the phonons disperse upwards away from the centre of the Brillouin zone. The D peak appears and increases in intensity following the Tuinstra and Koenig (TK) relation, $I(\text{D})/I(\text{G}) \propto 1/L_a$ [1]. Stage 2 is the introduction of topological disorder into the graphite layer. The bonding is still mainly sp^2 , but the weaker bonds soften the vibrational modes, so the G peak decreases to ~ 1510 cm^{-1} . The TK relation is no longer valid, but $I(\text{D})/I(\text{G}) \propto L_a^2$ [5], i.e. is proportional to the number of aromatic rings. Stage 3 is the conversion of

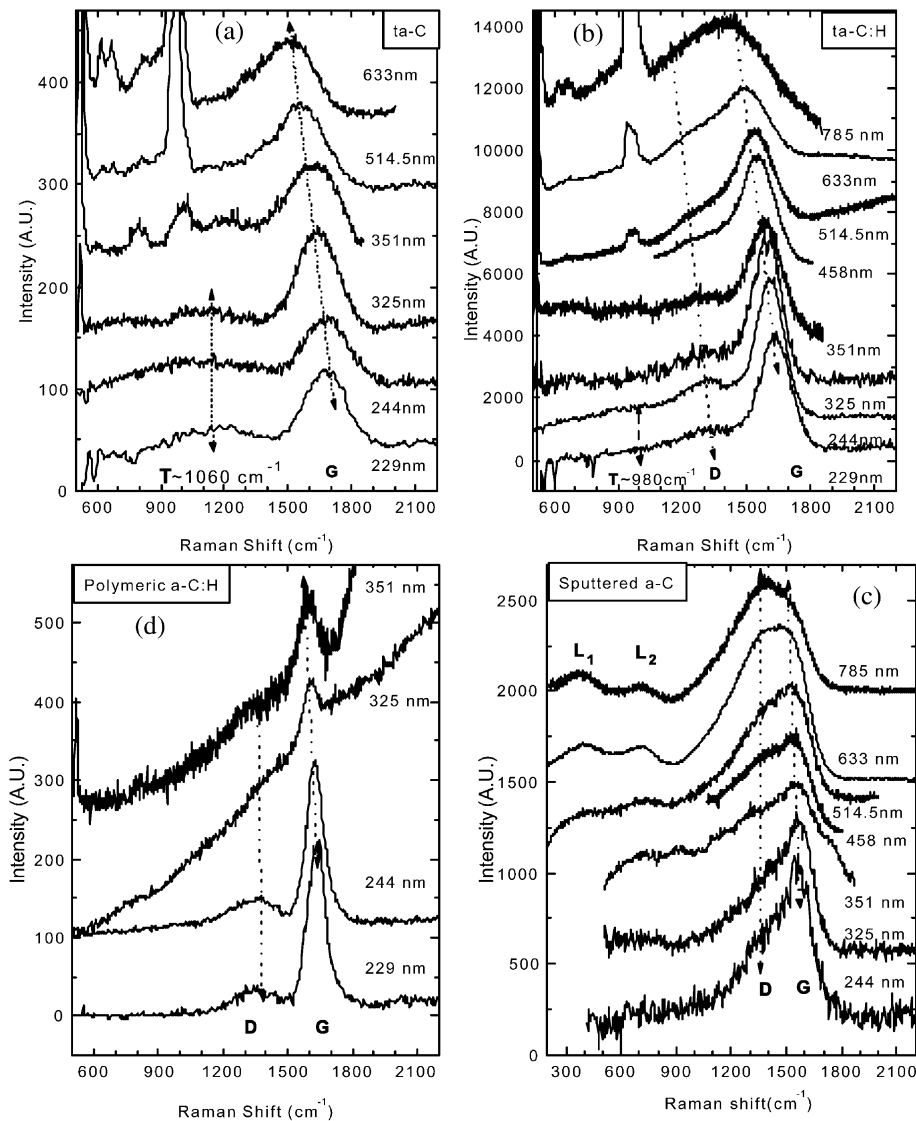


Fig. 1. MW Raman spectra of (a) ta-C, (b) ta-C:H, (c) sputtered a-C and (d) polymeric a-C:H. The peaks' trends and labels are indicated.

sp^2 sites to sp^3 sites and the consequent change of sp^2 configuration from rings to chains. The G peak position moves up to $\sim 1570\text{ cm}^{-1}$, due to the confinement of π electrons in shorter chains. $I(D)/I(G)$ is 0 due to the absence of rings.

We note that any features above $\sim 1360\text{ cm}^{-1}$ cannot be due to C–C sp^3 vibrations, being this the band limit for C–C sp^3 vibrations [5]. Thus, it is clear that the presence of G peaks in Fig. 1 means that sp^2 vibrations still dominate even for UV Raman excitation.

Fig. 3a shows the variation of the G peak position with excitation wavelength and energy. The G peak does not disperse in graphite itself, nanocrystalline (nc)-graphite or glassy carbon [26–29]. The G peak only disperses in more disordered carbon, where the dispersion is proportional to the degree of disorder. This is an important finding, by which the physical behaviour of

the G peak in disordered graphite is radically different from amorphous carbons, even though the G peak positions might accidentally be the same at some excitation energy. The G peak in graphite cannot disperse because it is the Raman-active phonon mode of the crystal. In nc-graphite, the G peak shifts slightly upwards at fixed excitation energy due to phonon confinement, but it cannot disperse with varying excitation energy, still being a density of states feature. The G peak dispersion occurs only in more disordered carbon, because now there are a range of configurations with different local band gaps and different phonon modes. The dispersion arises from a resonant selection of sp^2 configurations or clusters with wider π band gaps and, correspondingly, higher vibration frequencies. The G peak dispersion separates the materials into two types. In materials with only sp^2 rings, the G peak dispersion

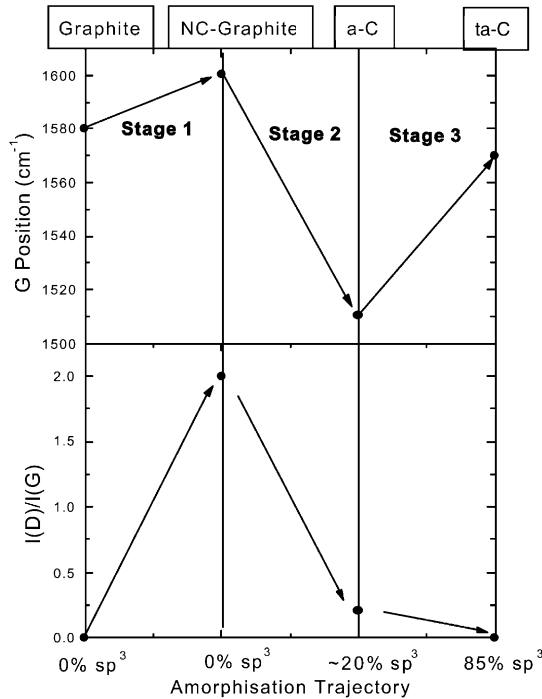


Fig. 2. Amorphisation trajectory, showing the schematic variation of G position and $I(D)/I(G)$ ratio for visible (514.5 nm) excitation [5].

saturates at a maximum of $\sim 1600 \text{ cm}^{-1}$, the G position in nc-graphite. In contrast, in those materials also containing sp^2 chains, particularly ta-C and ta-C:H, the G

peak continues to rise past 1600 cm^{-1} and can reach 1690 cm^{-1} at 229 nm excitation in ta-C. This high G peak position can only be due to short, strained $\text{C}=\text{C}$ bonded chains, if one notes that the $\text{C}=\text{C}$ stretching vibration in ethylene is at $\sim 1630 \text{ cm}^{-1}$.

Fig. 4a shows the variation of G position against the *amorphisation* trajectory, for four typical wavelengths. We pointed out [5] that following the reverse, *ordering* trajectory, from ta-C to graphite, there can be hysteresis. This means that there can be sp^2 clustering or π electron delocalisation without a corresponding $\text{sp}^2 \rightarrow \text{sp}^3$ conversion. For visible excitation, sp^2 clustering and ordering will always *raise* the G peak in stages 2 and 3. In contrast, in UV excitation, increasing clustering *lowers* the G position, as noted above. This is shown schematically in Fig. 4b. Comparing visible to UV excitation, there is an *inversion* of the trends [11]. This is another remarkable result, since it allows for a distinction of samples which, although having different structures, may accidentally show very similar Raman spectra at a certain wavelength.

4. The T peak and sp^3 content

The first UV Raman studies [30,31] found a new peak at $\sim 1060 \text{ cm}^{-1}$ labelled T. This peak is due to a resonant enhancement of the σ states, and it directly probes the sp^3 bonding. It corresponds to the peak in the CC sp^3 vibration density of states (VDOS) of ta-C

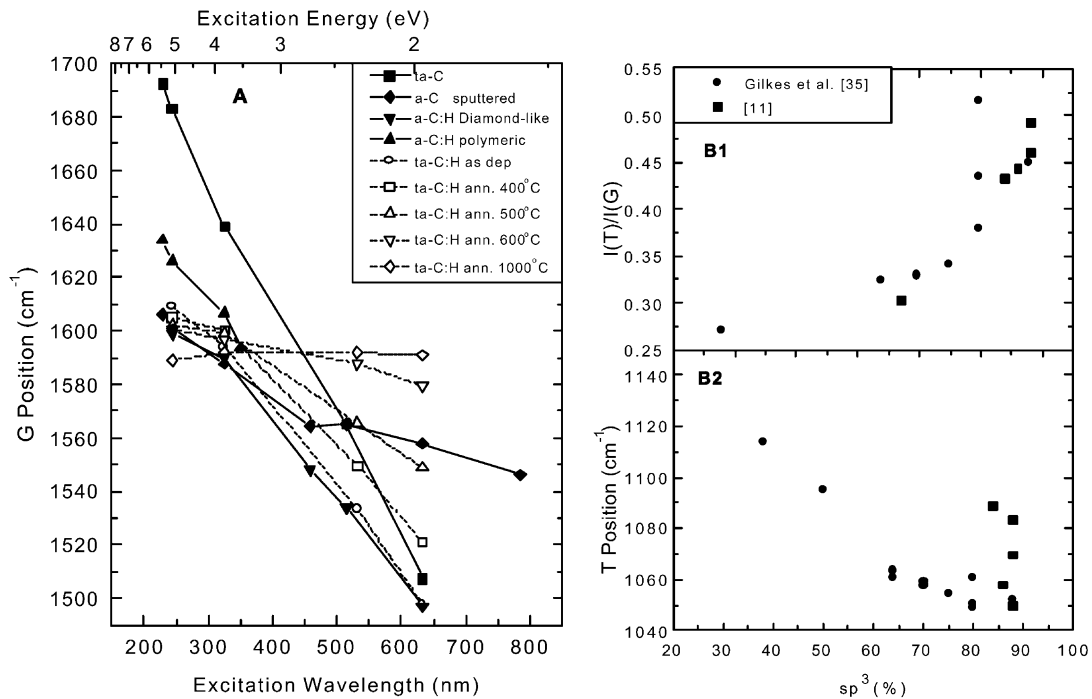


Fig. 3. (a) Dispersion of G peak vs. excitation wavelength, bottom x axis, and energy, top x axis, for a series of template samples. (B1,B2) $I(T)/I(G)$ and T peak position vs. sp^3 fraction for non-hydrogenated carbon films.

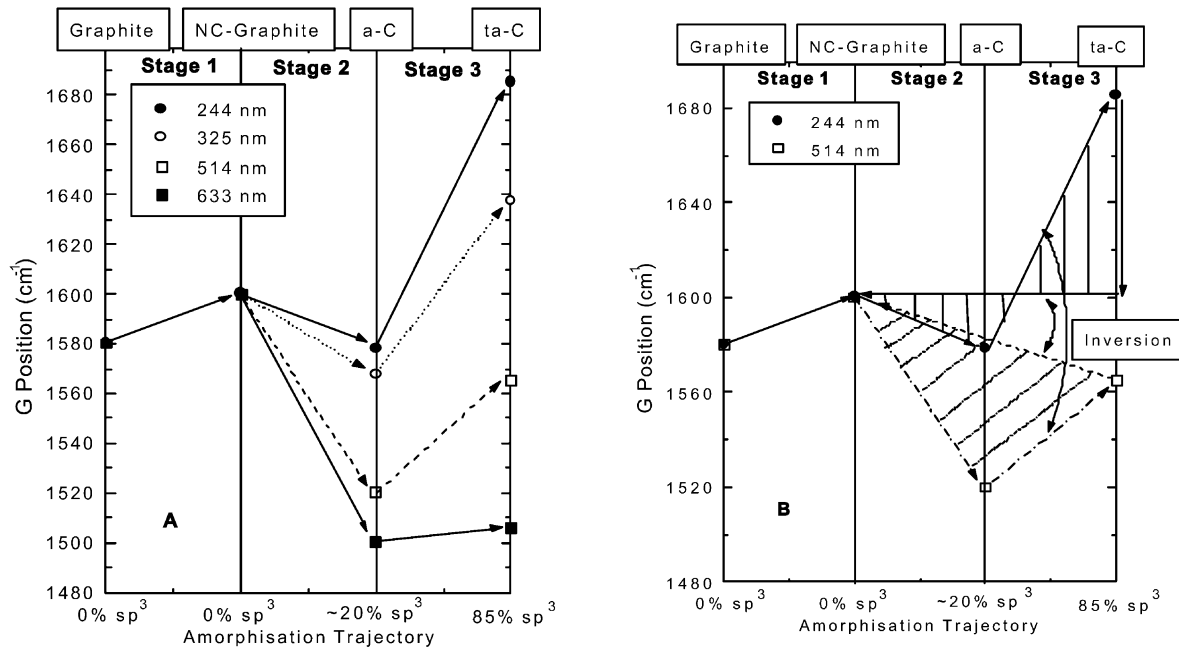


Fig. 4. (a) Amorphisation trajectory, showing the schematic variation of G peak position for four typical wavelengths; (b) amorphisation trajectory, showing the possibility of hysteresis in stages 2 and 3 for two typical wavelengths (514.5 and 244 nm). The regions span by hysteresis at 514.5 nm and 244 nm are evidenced by lines. Note the trend inversion, with the highest shift vis→UV for samples having the least ordered sp² phase.

in simulations [32,33] and EELS data [34]. Fig. 3b gives some empirical relations between the $I(T)/I(G)$ ratio, the T peak position and the sp³ content [35,11].

The 244 nm Raman spectrum is a favoured means to derive the sp³ content of amorphous carbons. This requires an understanding of how the spectrum develops with sp³ content. For example, the variation of $I(T)/I(G)$ with the sp³ content is quite non-linear for 60–90% sp³ contents, Fig. 3b1. The spectrum possesses the large G peak. If this is subtracted, this leaves the T peak, which arises from a peak in the sp³ VDOS. As the sp³ content falls, the VDOS peak at 1060 cm⁻¹ shifts upwards to that of a sp² network at 1400 cm⁻¹ [34]. Alternatively, the changes could be represented as a reduction of the T peak at 1060 cm⁻¹ and the rise of a peak at approximately 1400 cm⁻¹, a D-like peak. This is consistent with our finding that a D peak can survive in UV in sp² a-C, where it becomes like a VDOS feature of sp² rings [11]. Thus, as the sp² content of ta-C rises, the T peak intensity (corresponding to the CC sp³ VDOS) is reduced, with a corresponding increase of a D peak. A complication is that the D peak intensity depends not only on the sp² fraction, but also on its order. If the sp² sites have graphitic order, the D peak is absent in UV, if the sp² sites are in chains the D peak is absent, only if the sp² sites are in disordered rings does a residual D peak survive in UV [11]. This can then explain the range of $I(T)/I(G)$ values seen for high sp³ content ta-C.

The increase of sp² content and clustering both tend

to reduce the T peak intensity relative to the G peak. However, the T peak disappears only for large sp² contents. Thus, the effect of clustering is to reduce the direct correlation between T intensity and sp³ content. Nevertheless, we can still distinguish high sp³ contents from low sp³, unlike in visible Raman spectra. Indeed, a T peak at approximately 1060 cm⁻¹ and an $I(T)/I(G)$ ratio of approximately ~0.4–0.42 in H-free samples is a sufficient condition to estimate an sp³ content of ~80%. An $I(T)/I(G)$ ratio of 0.3–0.4 still indicates a sp³ content of 60–80%, but sp² clustering makes it difficult to give a precise figure. Finally, $I(T)/I(G) < 0.2$ indicates a sp³ content lower than 20–30%. Thus the presence of a T peak is a powerful qualitative means to cut through the hysteresis. Indeed, a sample with high sp³ fraction and large hysteresis will show a T peak (even if smaller than a similar sp³ content sample, but with limited clustering of the sp² phase). However, a sample with low sp³ fraction, but with the same $I(D)/I(G)$ in visible excitation, will not show any T peak in the UV.

The analysis of T peaks extends to hydrogenated samples. Fig. 1b shows that the T peak in ta-C:H or a-C:H is approximately ~980 cm⁻¹, lower than in ta-C. This is consistent with the simulations of the C–C sp³ VDOS in ta-C:H [36]. The presence of the residual D peak must be taken into account when fitting. For hydrogenated samples, EELS gives the total amount of sp³ bonded C atoms, both as C–C and C–H sp³ bonds, but the T peak is sensitive only to C–C sp³ bonds.

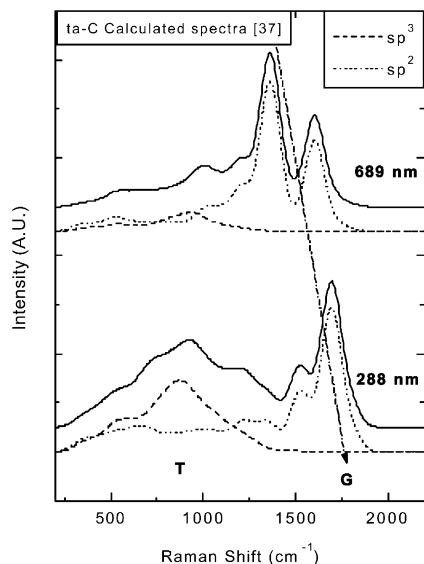


Fig. 5. Calculated Raman spectra for 1.8 and 4.3 eV excitation for a model ta-C sample [37]. The total Raman spectra are decomposed in the contributions from sp^2 and sp^3 atoms. The double peak structure of the G peak is an artefact due to the small number of sp^2 sites in the 64 atoms model ta-C. The G peak dispersion and the T peak are indicated.

Indeed, comparing the UV Raman spectra of ta-C:H and polymeric a-C:H (Fig. 1b,d), it is clear that most C sp^3 atoms are bonded to H in polymeric a-C:H, due to the absence of a clear T peak, whilst in ta-C:H there is a sizeable amount of C–C sp^3 bonds. Empirically, $I(T)/I(G) \sim 0.1–0.2$ in (t)a-C:H indicates an overall sp^3 content of $\sim 70\%$. Clearly, as sp^2 clustering also contributes to a D peak, this can make things more difficult.

Recently Profeta and Mauri provided the first calculation of the resonant Raman spectra of a model ta-C structure [37]. This is a major improvement, since so far we could only rely on calculated VDOS, which clearly fail to explain any resonant phenomenon. Fig. 5 shows the simulated Raman spectra for 1.8 eV and 4.3 eV excitation energies and the relative contribution of vibrations coming from sp^2 and sp^3 atoms [37]. The double structure of the G peak is an artefact due to the small number of sp^2 sites, organised as dimers and short chains (up to six atoms), in the 64-atom model. Anyway, Fig. 5 confirms that the T peak is really due to C–C sp^3 vibrations and that it only appears for UV excitation, whilst its contribution is negligible for visible excitation. Furthermore, as shown by the arrow, Fig. 5, gives a G peak dispersion consistent with that experimentally found. Further work on other samples with different sp^2 phase configurations is needed for more detailed conclusions. Profeta and Mauri [37] also showed that, for ~ 5 eV excitation, the sp^2 and sp^3 cross-sections are roughly the same. This verifies that 244 nm Raman

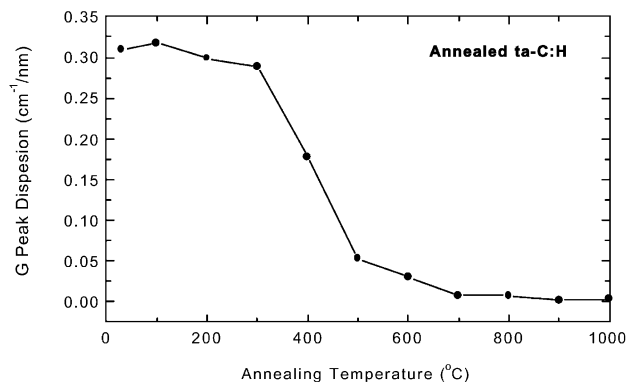


Fig. 6. G peak dispersion for annealed ta-C:H samples, from Fig. 3a.

gives an evenly weighted probe of the sp^2 and sp^3 phases. Only for energies higher than 6 eV the sp^3 C atoms would provide 90% of the total intensity. It would thus be of interest exploring such a high energy region.

5. A flavour of MW Raman capabilities

In the following subsections we will give some examples to show how the three-stage model for the G peak can be used, and how UV Raman can detect CH, CSi, SiH, and CN sp vibrations. We will not discuss in detail each example per se, since we just want to stress the capabilities of the MW Raman analysis.

5.1. Examples of the G peak dispersion

Fig. 6 plots the dispersion of the G peak for ta-C:H samples annealed at increasing temperatures. The drop

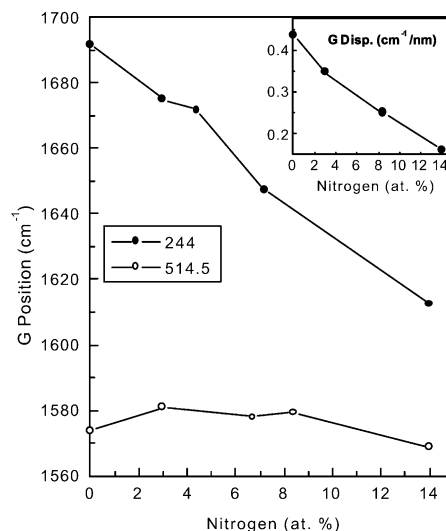


Fig. 7. G peak position (measured at 244 and 524.5 nm) vs. nitrogen content for ta-C:N samples deposited with a S-bend FCVA [40]. The insert shows the G peak dispersion vs. N content.

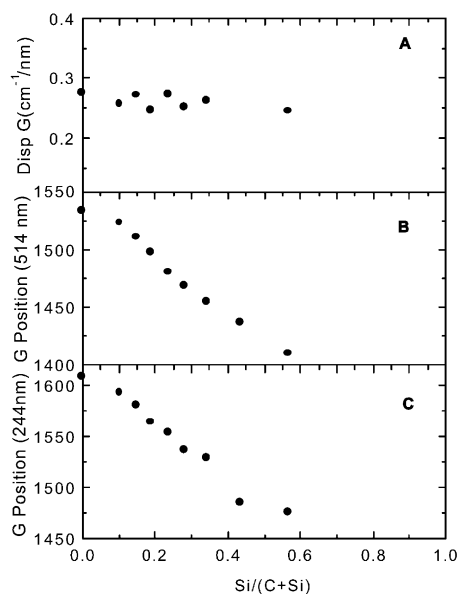


Fig. 8. Variation of (a) G peak dispersion, (b) 514.5 nm G position and (c) 244 nm G position for a series of (t)a-C_{1-x}Si_xH alloys as a function of $x = \text{Si}/(\text{C} + \text{Si})$.

of the G peak dispersion corresponds to the onset of the clustering of the sp² phase, just before the onset of sp³ to sp² conversion and H effusion [38,39].

Fig. 7 plots the G peak position measured for 514.5 and 244 nm excitations of a series of ta-C:N samples, with increasing N content, deposited with an S-Bend FCVA [40]. The G peak position is almost constant at 514.5 nm, with a very slight tendency to increase with N, but decreases linearly with N for 244 nm excitation. Indeed, the insert in Fig. 7 shows how the dispersion of the G peak decreases linearly with N. This is a nice example of what we called hysteresis and inversion in Fig. 4b. Due to hysteresis the G peak position does not change at 514.5 nm. The trend inversion with clustering, resulting in a smaller jump from green to UV the higher the clustering of the sp² phase, gives a linear decrease of G with N content and allows to resolve the ambiguity of the single wavelength study. It is also evident how, with a proper calibration, this can be a quick means to estimate the N content in amorphous carbon nitrides [41].

Vice-versa, Fig. 8 plots the G peak position and dispersion as a function of the Si/(Si+C) ratio for a series of (t)a-C_{1-x}Si_xH_y alloys [42]. For both green and UV excitations the G peak linearly downshifts with x , thus the dispersion of the G peak is constant with x . This means that an increase in the Si content does not increase the clustering of the sp² phase and no hysteresis happens. The Si content can then be directly derived for the G position in either green or UV Raman spectra [42].

5.2. Detecting heteroatoms vibrations in UV Raman

In Section 4 we pointed out how UV Raman spectra can detect the C–C σ bonds, due to the increase of their cross section with respect to the π bonds. Here we show that this is a general feature and also the σ bonds between heteroatoms can be clearly seen in UV excitation. This opens the way to using UV Raman spectroscopy as a complementary tool to IR spectroscopy for elemental detection.

Fig. 1d plotted the MW Raman spectra of polymeric a-C:H. Fig. 1d shows that for decreasing excitation energy the PL background increases and overshadows the Raman spectra. Indeed no Raman spectrum of polymeric a-C:H was so far reported, but rather meaningless straight lines [43]. UV Raman, if carefully performed to avoid damage, allows to get a spectrum of polymeric a-C:H and to correlate it with the film properties [11]. Furthermore, Fig. 9 plots the comparison of the second order spectral region of a polymeric a-C:H and a polymeric a-C:D. This shows that the ~ 2920 cm⁻¹ CH_x stretching modes can be detected in UV Raman, as confirmed by the downshift of this band to ~ 2100 – 2200 cm⁻¹ upon deuterium substitution [11].

Fig. 10 shows the MW Raman spectra of a ta-C:H:N with 26 at.% H and 29 at.% N [41]. In this figure the G peak heights are normalised to be the same at all excitation energies. The spectra and the insert demonstrate that the intensity ratio of the sp CN peak with respect to the G peak increases six times going from 514.5 to 244 nm excitation. Indeed, whilst it was not

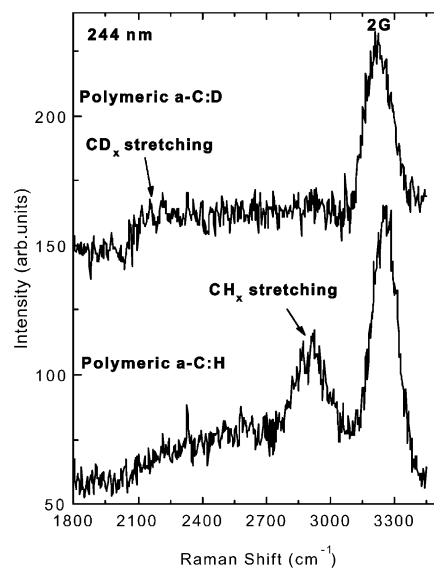


Fig. 9. Comparison of the second order region of the 244 nm Raman spectra of polymeric a-C:H and a-C:D samples. Note the downshift of the ~ 2920 cm⁻¹ band to ~ 2100 – 2200 cm⁻¹ upon deuteration, as expected for a C–H stretching.

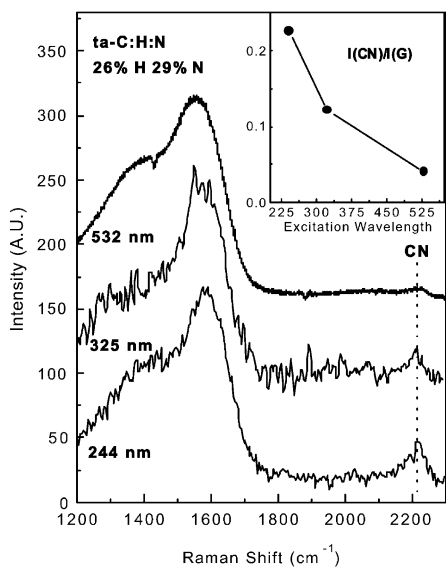


Fig. 10. MW Raman spectra of a ta-C:H:N sample with 26% H and 29% N. The insert shows the increase of the $I(\text{CN})/I(\text{G})$ ratio for increasing excitation energy.

possible to get a precise trend of $I(\text{CN})/I(\text{G})$ for a series of ta-C:H:N measured only at 514.5 excitation [44], the use of UV raman spectra allowed us to get a linear correlation between $I(\text{CN})/I(\text{G})$ and the N content [41].

Fig. 11 plots the MW Raman spectra of an amorphous carbon silicon alloy with $\text{Si}/(\text{C} + \text{Si}) = 0.35$. The UV Raman spectra show two extra features at ~ 760 and 960 cm^{-1} , corresponding to the peaks in the VDOS of SiC, as expected for an amorphous silicon carbide [45]. These peaks are almost never detected in visible Raman spectra of a-SiC alloys, due to the small cross-section of Si–C vibration.

Fig. 12 compares the IR and the UV Raman spectra of a a-Si:H film deposited at room temperature. The band at $\sim 2100 \text{ cm}^{-1}$ is thus identified as Si–H₂ stretching [46,42], and it is also seen in UV Raman spectra of the (t)a-C_{0.65}:Si_{0.35}:H alloy of Fig. 11. The band at $\sim 650 \text{ cm}^{-1}$ is due to SiH_n bending [46,42].

6. Conclusions

We have presented and reviewed the dispersion of Raman peaks with varying excitation energy for amorphous carbons. In particular we focused on the trends of the G peak, which can be classified and explained by extending to MW Raman the three-stage model developed to explain the visible Raman spectra of disordered and amorphous carbons.

We discussed the origin of the trends of the T peak with sp³ content for hydrogenated and hydrogen free samples.

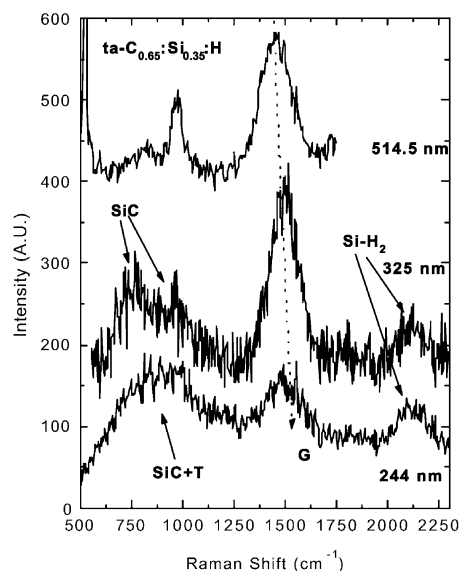


Fig. 11. MW Raman spectra of a ta-C_{0.65}:Si_{0.35}:H sample. For UV excitation the SiC modes and the Si–H₂ stretching are seen.

We stressed how the clustering of the sp² phase is the major parameter controlling the Raman spectra at any wavelength. Probing the same sample with visible and UV excitation allows us to derive the amount and clustering of sp² sites, at least qualitatively. This is due to the inversion of the trends of the G peak, resulting in a larger visible to UV shift for less sp² clustering. The appearance of the T peak gives a direct indication of the presence of sp³ bonds. This means that a two wavelength study (e.g. at 514 and 244 nm) can provide a fast and powerful characterisation tool for amorphous and disordered carbons since the peaks' dispersion is a

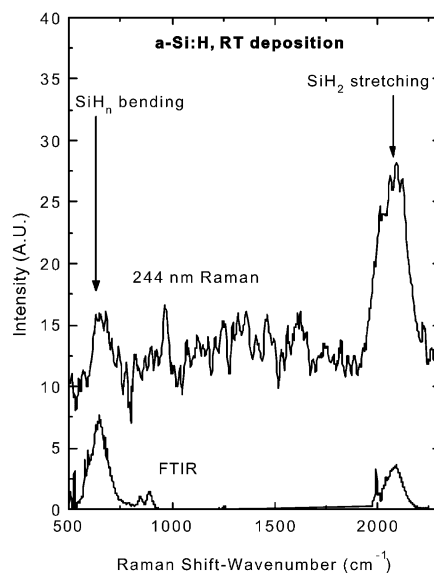


Fig. 12. Comparison of 244 nm Raman and FTIR spectra of an a-Si:H sample deposited at room temperature, with 30 at.% H.

fingerprint which is specific to each different carbon system.

In order to demonstrate the capabilities of MW Raman spectroscopy, we presented a series of key examples showing how to use the G peak dispersion for structural and elemental analysis and how UV Raman spectroscopy can easily detect the heteroatoms vibrations, in a complementary way to IR spectroscopy.

Acknowledgments

The author thanks John Robertson for guidance and fruitful discussions. The author acknowledges D. Batchelder of University of Leeds, M. Stutzmann of Walter Schottky Institut Muenchen, M. Kuball of University of Bristol, D. Richards of Cavendish Laboratory, Cambridge, D. Roy and B. Clyne of Materials Science and Metallurgy, Cambridge, and C.E. Bottani of Politecnico di Milano for the access to Raman facilities and kind hospitality in their laboratories. C. Castiglioni of Politecnico di Milano and F. Mauri of Université Pierre et Marie Curie of Paris for useful discussions. S.E. Rodil for a-C:D and (t)a-C:(H):N samples. Support from an European Union TMR Marie Curie fellowship and from Churchill College, Cambridge is gratefully acknowledged.

References

- [1] F. Tuinstra, J.L. Koenig, *J. Chem. Phys.* 53 (1970) 1126.
- [2] R.J. Nemanich, S.A. Solin, *Phys. Rev. B* 20 (1979) 329.
- [3] P. Lespade, A. Marchard, M. Couzi, F. Cruege, *Carbon* 22 (1984) 375.
- [4] M.A. Tamor, W.C. Vassel, *J. Appl. Phys.* 76 (1994) 3823.
- [5] A.C. Ferrari, J. Robertson, *Phys. Rev. B* 61 (2000) 14095.
- [6] A.M. Rao, E. Richter, S. Bandow, et al., *Science* 75 (1997) 187.
- [7] D.S. Bethune, G. Meijer, W.C. Tang, et al., *Chem. Phys. Lett.* 179 (1991) 181.
- [8] M.A. Pimenta, A. Marucci, S.A. Empedocles, et al., *Phys. Rev. B* 58 (1998) R16016.
- [9] S.D.M. Brown, P. Corio, A. Marucci, M.S. Dresselhaus, M.A. Pimenta, K. Kneipp, *Phys. Rev. B* 61 (2000) R5137.
- [10] A.G. Souza Filho, A. Jorio, J.H. Hafner, et al., *Phys. Rev. B* 63 (2001) R241404.
- [11] A.C. Ferrari, J. Robertson, *Phys. Rev. B* 64 (2001) 075414.
- [12] A.C. Ferrari, J. Robertson, *Phys. Rev. B* 63 (2001) R121405.
- [13] K. Ushizawa, K. Watanabe, T. Ando, et al., *Diamond Relat. Mater.* 7 (1998) 1719.
- [14] F. Pruvost, A. Deneuve, *Diamond. Relat. Mater.* 10 (2001) 531.
- [15] A. Otto, in: M. Cardona, G. Guntherodt (Eds.), *Light Scattering in Solids, IV*, Springer, Berlin, 1984.
- [16] M. Moskovits, *Rev. Mod. Phys.* 57 (1985) 783.
- [17] K. Kneipp, H. Kneipp, P. Corio, et al., *Phys. Rev. Lett.* 84 (2000) 3470.
- [18] G.S. Dusberg, W.J. Blau, H.J. Byrne, J. Muster, M. Burghard, S. Roth, *Chem. Phys. Lett.* 310 (1999) 8.
- [19] T. Lopez-Rios, E. Sandre, S. Leclercq, E. Sauvain, *Phys. Rev. Lett.* 76 (1996) 4935.
- [20] D.S. King, R. Weimer, L. Piloni, W.B. White, *Appl. Phys. Lett.* 56 (1990) 1320.
- [21] M.G. Beghi, A.C. Ferrari, C.E. Bottani, A. LiBassi, B.K. Tanner, J. Robertson, *Diamond Relat. Mater.*, in press.
- [22] D.W. Pohl, W. Derik, M. Lanz, *Appl. Phys. Lett.* 44 (1984) 651.
- [23] S. Webster, D.N. Batchelder, D.A. Smith, *Appl. Phys. Lett.* 72 (1998) 1478. K.J. Baldwin, D.N. Batchelder, S. Webster, *Raman Microscopy: Confocal and Scanning Near-Field*, in: I.R. Lewis, G.M. Edwards, (Eds.), *Handbook of Raman Spectroscopy*, Marcel Dekker, Inc., New York, 2001, p. 145.
- [24] V. Deckert, et al., *Chem. Phys. Lett.* 318 (2000) 131.
- [25] A.C. Ferrari, A. Libassi, B.K. Tanner, et al., *Phys. Rev. B* 62 (2000) 11089.
- [26] R.P. Vidano, D.B. Fishbach, L.J. Willis, T.M. Loehr, *Solid. State Commun.* 39 (1981) 341.
- [27] K. Sinha, J. Menendez, *Phys. Rev. B* 41 (1990) 10845.
- [28] Y. Wang, D.C. Alsmeyer, R.L. McCreery, *Chem. Mater.* 2 (1990) 557.
- [29] I. Pocsik, M. Koos, M. Hundhausen, L. Ley, in: S.R.P. Silva, et al. (Eds.), *Amorphous Carbon: State of the Art*, World Scientific, Singapore, 1998, p. 224.
- [30] K.W.K. Gilkes, H.S. Sands, D.N. Batchelder, J. Robertson, W.I. Milne, *Appl. Phys. Lett.* 70 (1980) 1997.
- [31] V.I. Merkulov, J.S. Lannin, C.H. Munro, S.A. Asher, V.S. Veerasamy, W.I. Milne, *Phys. Rev. Lett.* 78 (1997) 4869.
- [32] T. Kohler, T. Frauenheim, G. Jungnickel, *Phys. Rev. B* , 52 (1995) 11837.
- [33] D.A. Drabold, P.A. Fedders, P. Strumm, *Phys. Rev. B* 49 (1994) 16415.
- [34] G.P. Lopinski, V.I. Merkulov, J.S. Lannin, *Appl. Phys. Lett.* 69 (1996) 3348.
- [35] K.W.R. Gilkes, S. Praver, K.W. Nugent, et al., *J. Appl. Phys.* 87 (2000) 7283.
- [36] F. Mauri, A. Del Corso, *Appl. Phys. Lett.* 75 (1999) 644.
- [37] M. Profeta, F. Mauri, *Phys. Rev. B* 63 (2001) 245415.
- [38] N.M.J. Conway, A.C. Ferrari, A.J. Flewitt, et al., *Diamond Relat. Mater.* 9 (2000) 765.
- [39] A. Ilie, A.C. Ferrari, T. Yagi, J. Robertson, *Appl. Phys. Lett.* 76 (2000) 2627.
- [40] M.C. Polo, J.L. Andujar, A. Hart, J. Robertson, W.I. Milne, *Diamond Relat. Mater.* 9 (2000) 633.
- [41] A.C. Ferrari, S.E. Rodil, J. Robertson, unpublished.
- [42] B. Racine, A.C. Ferrari, N.A. Morrison, I. Hutchings, W.I. Milne, J. Robertson, *J. Appl. Phys.* 90 (2001) 5002.
- [43] Q. Zhang, S.F. Yoon, Rusli, J. Ahn, H. Yang, D. Bahr, *J. Appl. Phys.* 84 (1998) 5538.
- [44] S.E. Rodil, A.C. Ferrari, J. Robertson, W.I. Milne, *J. Appl. Phys.* 89 (2001) 5425.
- [45] K. Karch, P. Pavone, W. Windl, O. Shutt, D. Strauch, *Phys. Rev. B* 50 (1994) 17045.
- [46] G. Lucovsky, R.J. Nemanich, J. Knights, *Phys. Rev. B* 19 (1979) 2064.